D-Ribulose 5-Phosphate 3-Epimerase: Functional and Structural Relationships to Members of the Ribulose-Phosphate Binding $(\beta/\alpha)_8$-Barrel Superfamily[†,‡]

Julie Akana,[§] Alexander A. Fedorov,[||] Elena Fedorov,[||] Walter R. P. Novak,[⊥] Patricia C. Babbitt,[⊥] Steven C. Almo,*[,||,⊥] and John A. Gerlt*[,§]

Departments of Biochemistry and Chemistry, University of Illinois at Urbana−Champaign, 600 S. Mathews Avenue, Urbana, Illinois 61801, Departments of Biochemistry and Physiology and Biophysics, Albert Einstein College of Medicine, Bronx, New York 10461, and Departments of Biopharmaceutical Sciences and Pharmaceutical Chemistry, University of California, San Francisco, California 94143

Received December 3, 2005; Revised Manuscript Received January 6, 2006

ABSTRACT: The "ribulose phosphate binding" superfamily defined by the Structural Classification of Proteins (SCOP) database is considered the result of divergent evolution from a common $(\beta/\alpha)_8$-barrel ancestor. The superfamily includes D-ribulose 5-phosphate 3-epimerase (RPE), orotidine 5′-monophosphate decarboxylase (OMPDC), and 3-keto-L-gulonate 6-phosphate decarboxylase (KGPDC), members of the OMPDC suprafamily, as well as enzymes involved in histidine and tryptophan biosynthesis that utilize phosphorylated metabolites as substrates. We now report studies of the functional and structural relationships of RPE to the members of the superfamily. As suggested by the results of crystallographic studies of the RPEs from rice [Jelakovic, S., Kopriva, S., Suss, K. H., and Schulz, G. E. (2003) *J. Mol. Biol. 326*, 127−35] and *Plasmodium falciparum* [Caruthers, J., Bosch, J., Bucker, F., Van Voorhis, W., Myler, P., Worthey, E., Mehlin, C., Boni, E., De Titta, G., Luft, J., Kalyuzhniy, O., Anderson, L., Zucker, F., Soltis, M., and Hol, W. G. J. (2006) *Proteins 62*, 338−42], the RPE from *Streptococcus pyogenes* is activated by Zn^{2+} which binds with a stoichiometry of one ion per polypeptide. Although wild type RPE has a high affinity for Zn^{2+} and inactive apoenzyme cannot be prepared, the affinity for Zn^{2+} is decreased by alanine substitutions for the two histidine residues that coordinate the Zn^{2+} ion (H34A and H67A); these mutant proteins can be prepared in an inactive, metal-free form and activated by exogenous Zn^{2+}. The crystal structure of the RPE was solved at 1.8 Å resolution in the presence of D-xylitol 5-phosphate, an inert analogue of the D-xylulose 5-phosphate substrate. This structure suggests that the 2,3-enediolate intermediate in the 1,1-proton transfer reaction is stabilized by bidentate coordination to the Zn^{2+} that also is liganded to His 34, Asp 36, His 67, and Asp 176; the carboxylate groups of the Asp residues are positioned also to function as the acid/base catalysts. Although the conformation of the bound analogue resembles those of ligands bound in the active sites of OMPDC and KGPDC, the identities of the active site residues that coordinate the essential Zn^{2+} and participate as acid/base catalysts are not conserved. We conclude that only the phosphate binding motif located at the ends of the seventh and eighth β-strands of the $(\beta/\alpha)_8$-barrel is functionally conserved among RPE, OMPDC, and KGPDC, consistent with the hypothesis that the members of the "ribulose phosphate binding" $(\beta/\alpha)_8$-barrel "superfamily" as defined by SCOP have not evolved by evolutionary processes involving the intact $(\beta/\alpha)_8$-barrel. Instead, this "superfamily" may result from assembly from smaller modules, including the conserved phosphate binding motif associated with the C-terminal $(\beta/\alpha)_2$-quarter barrel.

The $(\beta/\alpha)_8$-barrel is the most commonly observed fold in structurally characterized enzymes (*1*−*3*). The most recent release (1.69; July 2005) of the Structural Classification of Proteins database (SCOP; http://scop.mrc-lmb.cam.ac.uk/scop/) lists 31 "superfamilies" that share this fold. The reactions catalyzed by the members of the various superfamilies are mechanistically varied: some are cofactor-independent, e.g., the prototypic triose phosphate isomerase; some require metal ions, e.g., the members of the mechanistically diverse enolase and amidohydrolase superfamilies; and others require organic cofactors, e.g., pyridoxal-phosphate dependent enzymes. The observation that the active sites of these enzymes are always formed by residues located at the C-terminal ends of the various β-strands has led to the suggestion that many (perhaps all?) of the superfamilies identified in SCOP were derived from a common progenitor via divergent evolution.

A particularly interesting superfamily in SCOP is designated the "ribulose phosphate binding" superfamily. The

[†] This research was supported by Grant GM-65155 (to J.A.G. and S.C.A.) from the National Institutes of Health.

[‡] The X-ray coordinates and structure factors for the D-xylitol·Zn^{2+} complex of RPE have been deposited in the Protein Data Bank (PDB accession code, 2FLI).

* To whom correspondence should be addressed. J.A.G.: Department of Biochemistry, University of Illinois, 600 S. Mathews Avenue, Urbana, IL 61801; phone (217) 244-7414; fax (217) 244-6538; e-mail j-gerlt@uiuc.edu. S.C.A.: Department of Biochemistry, Albert Einstein College of Medicine, 1300 Morris Park Avenue, Bronx, NY 10461; phone (718) 430-2746; fax (718) 430-8565; e-mail almo@aecom.yu.edu.

[§] University of Illinois at Urbana−Champaign.

[||] Albert Einstein College of Medicine.

[⊥] University of California.

10.1021/bi052474m CCC: $33.50
Published on Web 02/02/2006

members of this superfamily catalyze diverse reactions and include the following families:

(1) Phosphoribosylformimino-5-aminoimidazole carboxamide ribotide isomerase (HisA) and imidazoleglycerolphosphate synthase (HisF), enzymes that catalyze successive steps in histidine biosynthesis. Sterner and Wilmanns and their co-workers have established that HisA, that catalyzes an Amadori rearrangement, and HisF, that catalyzes the Gln-dependent (NH_3) formation of the imidazole functional group, are dimers of homologous $(\beta/\alpha)_4$-half barrels (*4*, *5*). An Asp at the end of the first β-strand in each half barrel is essential for catalysis, with these likely participating as acid/base catalysts.

(2) *N*-(5′-Phosphoribosyl)anthranilate isomerase (PRAI), indole-3-glycerophosphate synthase (IGPS), and the α-subunit of tryptophan synthase (αTS), enzymes that catalyze three successive reactions in tryptophan biosynthesis. PRAI catalyzes an Amadori rearrangement analogous to that catalyzed by HisA; in fact, in some organisms a single protein catalyzes both the HisA and PRAI reactions. Given this natural functional promiscuity, the report from Sterner and co-workers that single amino acid substitutions in HisA are sufficient to introduce PRAI activity, thereby generating unnatural functional promiscuity, is not unexpected (*6*). Although IGPS and αTS share the $(\beta/\alpha)_8$-barrel fold with HisA, HisF, and PRAI, they share no discernible sequence similarity with one another or the other enzymes in the His and Trp biosynthetic pathways.

(3) "Decarboxylases" that catalyze mechanistically distinct reactions. The most ubiquitous member of this family is the metal ion/cofactor-independent orotidine 5′-monophosphate decarboxylase (OMPDC[1]) in pyrimidine biosynthesis. The OMPDC-catalyzed reaction continues to attract considerable attention because the enzyme must avoid the formation of a highly unstable vinyl anion intermediate (*7*); however, the strategy by which this is accomplished is not yet unequivocally established (*8*−*10*). We recently reported that two other enzymes are homologues of OMPDC, although they catalyze reactions that involve the Mg^{2+}-dependent stabilization of an enolate anion intermediate: 3-keto-L-gulonate decarboxylase (KGPDC) that catalyzes the formation of L-xylulose 5-phosphate and carbon dioxide in the anaerobic catabolism of L-ascorbate by *Escherichia coli* and other eubacteria; and D-*arabino*-hex-3-ulose 6-phosphate synthase (HPS) that catalyzes the aldol condensation of D-ribulose 5-phosphate and formaldehyde in the assimilation of formaldehyde by some eubacteria and archaea (*11*). We designated OMPDC, KGPDC, and HPS as members of the OMPDC suprafamily: although their active sites are located at a conserved dimer interface and share identical functional groups, the functional groups perform distinct functions in OMPDC and the Mg^{2+}-dependent enzymes. In fact, our mechanistic and structural analyses of the KGPDC-catalyzed decarboxylation reaction have established that the mechanisms of the OMPDC- and KGPDC-catalyzed reactions share *no* mechanistic features (*12*−*15*).

(4) D-Ribulose-5-phosphate 3-epimerase (RPE) that catalyzes the interconversion of D-ribulose 5-phosphate and D-xylulose 5-phosphate in both the reductive and oxidative pentose phosphate pathways. Despite the ubiquitous occurrence of these pathways, few mechanistic studies have been reported for RPE (*16*). Structures are available for RPEs from potato (*17*), rice (*18*), *Synechocystsis* (*19*), and *Plasmodium falciparum* (*20*), but none of these were determined in the presence of an active site ligand.

Despite their functional differences, the members of the four families of the ribulose phosphate binding superfamily share a conserved phosphate binding motif located at the ends of the seventh and eighth β-strands (*21*). In HisA and HisF that are formed from two homologous $(\beta/\alpha)_4$-half barrels, a phosphate binding motif is also located at the ends of the third and fourth β-strands (*5*). The substrates for the HisA- and HisF-catalyzed reactions are bisphosphorylated, with one phosphate group occupying each of the phosphate binding motifs.

Sterner, Wilmanns, and co-workers have convincingly demonstrated that HisA and HisF are formed from two (homologous) $(\beta/\alpha)_4$-half barrels (*5*). With the realization that a $(\beta/\alpha)_2$-quarter barrel is the smallest repeating unit in the intact $(\beta/\alpha)_8$-barrel (*2*, *22*, *23*), the functionally diverse members of the ribulose phosphate binding superfamily could be the result of combinatorial assembly of a $(\beta/\alpha)_2$-quarter barrel that provides the phosphate binding motif and one or more $(\beta/\alpha)_{2N}$-units (where $N = 1$, 2, or 3) that provide the catalytic residues. If such an assembly process is correct, the grouping of all four families in a single "ribulose phosphate binding" superfamily would improperly reflect the range of divergent evolution of structure and function.

The inclusion of RPE in the OMPDC suprafamily is subject to several caveats that require additional, careful sequence-, function-, and structure-based studies. First, proteins that share the $(\beta/\alpha)_8$-barrel fold have the same topology (cylindrical), so conserved residues may be required for attainment of the fold and not for enzymatic function. Second, active site functional groups are always located at the ends of the various β-strands in the $(\beta/\alpha)_8$-barrel, so the occurrence of catalytically important but different functional groups at the ends of specific β-strands may be fortuitous. And, third, the expectation that the active site must be contained within the cavity delimited by the ends of the various β-strands and the loops that connect these with the following α-helices may restrict the geometry of substrate binding, especially considering that the phosphate groups of the various substrates are constrained to be located in the canonical binding motifs that always occur at the ends of the seventh and eighth β-strands.[2]

In this article, we report the results of biochemical experiments that establish that a single Zn^{2+} ion is required for catalysis by the RPE from *Streptococcus pyogenes*. We also report the structure of this RPE with D-xylitol 5-phosphate, a stable analogue of the D-xylulose 5-phosphate product, bound in the active site. As suggested by structural studies of the RPE from rice (*18*) and *P. falciparum* (*20*), this structure includes a single Zn^{2+} ion coordinated to (1)

[1] Abbreviations: KGPDC, 3-keto-L-gulonate 6-phosphate decarboxylase; OMPDC, orotidine 5′-monophosphate decarboxylase; RPE, D-ribulose 5-phosphate 3-epimerase.

[2] If the $(\beta/\alpha)_8$-barrels of the ribulose phosphate binding superfamily were combinatorially constructed from independent $(\beta/\alpha)_N$-units (where $N = 1$, 2, or 3), the conserved location of the phosphate binding motif at the end of the seventh and eighth β-strands (the C-terminal $(\beta/\alpha)_2$-module) in IGPS, αTS, RPE, and the members of the OMPDC suprafamily likely requires an additional evolutionary explanation.

the 2- and 3-OH groups of the substrate analogue; (2) two strictly conserved His residues located at the ends of the second and third β-strands; and (3) two strictly conserved Asp residues located at the ends of the second and seventh β-strands that are the likely candidates for the acid/base catalysts in the 1,1-proton transfer reaction. Based on comparisons of these structure−function relationships with those previously established for both OMPDC (*8*) and KGPDC (*13*, *14*), we conclude that RPE and the homologous OMPDC and KGPDC are very distantly related, with the similarities resulting from the conserved phosphate binding motif at the ends of the seventh and eighth β-strands. Taken together, our analyses support the conclusion that RPE and the OMPDC suprafamily should be considered distinct superfamilies of $(\beta/\alpha)_8$-barrel proteins, as are several other superfamilies defined by SCOP (including triose phosphate isomerase) that share the conserved phosphate binding motif associated with the C-terminal $(\beta/\alpha)_2$-quarter barrel.

MATERIALS AND METHODS

Cloning, Expression, and Purification of Wild Type RPE. The gene encoding RPE was PCR-amplified from *S. pyogenes* SF370 genomic DNA purchased from the American Type Culture Collection; the primers encoded an *Nde*I restriction site at the 5′-end and an *Xho*I restriction site at the 3′-end of the gene. Following restriction, the gene was ligated into a modified version of pET15b that encodes an N-terminal 10-His tag.

The gene encoding RPE was expressed in the *Escherichia coli* strain BL21 (DE3) grown at 37 °C in LB with 100 μg/mL ampicillin to an optical density of 2 at 600 nm. The cells were collected by centrifugation, resuspended in binding buffer (5 mM imidazole, 0.5 M NaCl, 20 mM Tris-HCl, pH 7.9), and lysed by sonication. The lysate was applied to a chelating Sepharose Fast Flow column (Pharmacia Biotech) charged with Ni^{2+}. The column was washed with 15% elution buffer (1 M imidazole, 0.5 M NaCl, 20 mM Tris-HCl, pH 7.9)/85% wash buffer (60 mM imidazole, 0.5 M NaCl, 20 mM Tris-HCl pH 7.9), and the protein was eluted with 50% wash buffer/50% strip buffer (100 mM EDTA, 0.5 M NaCl, 20 mM Tris HCl pH 7.9). The N-terminal His tag was removed by thrombin cleavage (Pharmacia Biotech) according to the manufacturer's instructions. The protein was dialyzed into 10 mM Tris HCl, pH 7.9 and concentrated to 6−8 mg/mL.

Insertional Disruption of the Gene Encoding RPE. The method of Datsenko and Wanner (*24*) was used to construct an insertional deletion of the gene encoding RPE in *E. coli* strain BW25113. A fragment encoding kanamycin resistance replaced the middle 570 bp in the ~650 bp gene encoding RPE; this strain is designated *rpe*::kan. The desired junctions between the chromosomal DNA and insert were verified by DNA sequence analysis. This *rpe*::kan strain was used for expression and purification of mutant versions of RPE to prevent contamination by the chromosomally encoded RPE.

Construction and Purification of Mutants. The H34A, D36A, H67A, and D176A mutants were constructed by the overlap extension method. The resulting PCR products were digested with *Nde*I and *Xho*I and ligated into a derivative of the pDMS1a vector which encodes an N-terminal 10-His tag (*25*). The mutant plasmids so obtained were transformed into *rpe*::kan strain of *E. coli* described in the previous section. The transformed cells were grown as described for expression of the wild type RPE in strain BL21 (DE3) except that the medium also contained 50 μg/mL of kanamycin. The procedure previously described for purification of wild type RPE was used to obtain the mutant proteins.

Preparation of Metal-Free Enzymes. To remove adventitious divalent metal ions, water and buffers were stirred with Chelex-100 (5 g/L) overnight; plasticware was soaked in 10 mM sodium EDTA, pH 7.5, overnight and rinsed with metal-free water; and glassware was acid-washed in 1:1 nitric acid: sulfuric acid, rinsed with 10 mM sodium EDTA, pH 7.5, soaked overnight in 10 mM sodium EDTA, pH 7.5, and rinsed with metal-free water.

Divalent metal ions were removed from wild type RPE as follows. A solution of enzyme was concentrated to a volume of 2 mL in an Amicon ultrafiltration apparatus. The solution was diluted with 50 mL of 50 mM sodium EDTA in 10 mM sodium HEPES, pH 7.5, and concentrated to a volume of 2 mL; this procedure was repeated four times. The concentrated solution was then diluted with 50 mL of 10 mM sodium HEPES, pH 7.5, and concentrated to a volume of 2 mL; this procedure was repeated four times. Residual EDTA was then removed from the concentrated sample by gel filtration using a prepacked PD-10 column (Amersham) that had been washed with and equilibrated in metal-free 10 mM sodium HEPES, pH 7.5.

Divalent metal ions were removed from the H34A, D36A, H67A, and D176A mutants by dialysis against 1 L of 10 mM sodium HEPES, pH 7.5, containing 5 g/L of Chelex-100. After three changes of the dialysis solution, the samples were subjected to gel filtration using a prepacked PD-10 column as described in the previous paragraph.

*Reconstitution of Wild Type and Mutant RPE*s. The various proteins were separately incubated at concentrations of 25 μM (0.62 mg/mL) with varying concentrations of $ZnCl_2$ in a solution of 50 mM sodium HEPES, pH 7.5, containing 20 mM L-glutamate, 20 mM L-arginine, and 20% glycerol. If the Glu, Arg, and/or glycerol were omitted from these incubations, a significant amount of protein precipitated. After incubation, the samples were subjected to gel filtration using a prepacked PD-10 column equilibrated in metal-free 50 mM sodium HEPES, pH 7.5. After reconstitution and gel filtration, the proteins were soluble and stable.

Metal Ion Analyses. Inductively coupled plasma emission spectroscopy (ICP) data were obtained by the Garratt-Callahan Company, Burlingame, CA. The samples (1−7 mg/mL) were analyzed for 22 elements: Al, Ba, Be, Cd, Ca, Cr, Co, Cu, Fe, Pb, Li, Mg, Mn, Mo, Ni, K, Si, Ag, Na, Sr, V, and Zn.

A colorimetric assay using the 4-(2-pyridylazo)resorcinal (PAR) reagent was routinely employed for Zn analyses following reconstitution of metal-free proteins (*26*). Standard solutions of $ZnCl_2$ (0−10 μM) or a 5 μM sample of protein was mixed with 4 M guanidine HCl in 20 mM sodium HEPES, pH 7.5, and incubated at room temperature for 3 min. A solution of 100 μM PAR in 20 mM sodium HEPES, pH 7.5, was added, and the absorbance of the PAR−Zn complex at 500 nm was recorded.

Preparation of D-Ribulose 5-Phosphate and D-Xylulose 5-Phosphate. D-Ribulose 5-phosphate as prepared as previously described (*27*).

D-Xylulose 5-phosphate was synthesized enzymatically from D-xylose utilizing the successive actions of xylose isomerase and xylulokinase. The reaction mixture (250 mL) contained 40 mM D-xylose (13 mmol), 0.19 mM ATP, 13 mM (7 mmol) acetyl phosphate, 0.66 mM $MgCl_2$, 200 units of xylose isomerase from *E. coli*, 200 units of xylulokinase from *E. coli*, and 200 units of acetate kinase (Sigma) in 50 mM sodium maleate, pH 7.0. The reaction was allowed to proceed for 4 h at room temperature. Nucleotides were removed by filtration through a bed of activated charcoal and Celite; enzymes were removed by ultrafiltration. D-Xylulose 5-phosphate was purified by passing the resulting solution through a column of DEAE Sepharose Fast Flow (HCO_3^- form) and eluting the product with a gradient of triethylammonium bicarbonate (pH 8.0). Fractions containing the product were pooled, and triethylammonium bicarbonate was removed by evaporation. ^{1}H NMR (D_2O, 500 MHz): δ 4.4 (q, $J = 63.8$ Hz, 2H), δ 4.352 (d, $J = 2.26$ Hz, 1H), δ 4.01 (dt, $J = 6.49$ Hz, 1H), δ 3.65 (m, 2H). ^{13}C NMR (D_2O, 500 MHz): δ 172.397, δ 81.468, δ 75.189, δ 66.052, δ 63.579.

Preparation of D-Xylitol 5-Phosphate. D-Xylitol 5-phosphate was prepared from xylitol using xylulokinase from *E. coli*. The reaction (250 mL) contained 40 mM D-xylitol (Sigma), 0.75 mM ATP, 32 mM acetyl phosphate, 13 mM $MgCl_2$, 400 units of acetate kinase (Sigma), and 200 units of xylulokinase in 50 mM sodium maleate, pH 7. After 4 h at room temperature, the solution was filtered through Celite and activated charcoal to remove nucleotides; the enzymes were removed by ultrafiltration. D-Xylitol 5-phosphate was purified by passing the resulting solution through a column of DEAE Sepharose Fast Flow (HCO_3^- form) and eluting the product with a gradient of triethylammonium bicarbonate (pH 8.0). Fractions containing the product were pooled, and triethylammonium bicarbonate was removed by evaporation. ^{1}H NMR (D_2O, 500 MHz): δ 3.71 (m, 4H), δ 3.574 (m, 2H), δ 3.5 (m, 1H). ^{13}C NMR (D_2O, 500 MHz): δ 72.006, δ 71.273, δ 70.886, δ 64.976, δ 62.686.

Coupled-Enzyme Assay of RPE Activity. The production of D-xylulose 5-phopshate from D-ribulose 5-phosphate catalyzed by RPE was quantitated with an irreversible, coupled-enzyme, continuous spectrophotometric assay (*28*). The assay (0.2 mL) contained D-ribulose 5-phosphate (0.0625−20 mM), 50 mM glycolaldehyde, 0.1 mM thiamin pyrophosphate, 0.16 mM NADH, 20 μg of transketolase, 4 units of triose phosphate isomerase, 2 units of glycerolphosphate dehydrogenase, and 10 mM $MgCl_2$ in 50 mM sodium HEPES, pH 7.5. The change in absorbance at 340 nm was measured, with the measured value representing the rate of conversion of D-ribulose 5-phosphate to D-xylulose 5-phosphate.

Polarimetric Assay of RPE Activity. A polarimeter-based assay of RPE activity was also used to avoid contamination with divalent metal ions. Because D-ribulose 5-phosphate and D-xylulose 5-phosphate have significantly different optical rotations at 589 nm, the rate of formation of their equilibrium mixture can be quantitated by measuring the change in optical rotation. In contrast to the irreversible spectrophotometric assay described in the previous section, the rate measured in the reversible polarimetric assay is the sum of the values of the forward (e.g., D-ribulose 5-phosphate to D-xylulose 5-phosphate) and reverse (D-xylulose 5-phosphate to D-ribulose 5-phosphate) rate constants (*29*). The assay (1.3 mL) contained 10 mM D-ribulose 5-phosphate (or 10 mM D-xylulose 5-phosphate) in 10 mM sodium HEPES, pH 7.5, in a 100 mm path length cuvette. The optical rotation at 589 nm was recorded as a function of time at room temperature using a Jasco P-1010 polarimeter and a sodium light source. Adventitious divalent metal ions were removed from the cuvette by soaking in a 1:1 mixture of nitric and sulfuric acids for 15 min, rinsing with metal-free water, and soaking overnight in 50 mM sodium EDTA, pH 7.5; the cuvette was rinsed with metal-free water before use. Values of [α] of 28.24° for D-ribulose 5-phosphate and of 4.9° for D-xylulose 5-phosphate were used to quantitate the rates of product formation.

Crystallization and Data Collection. RPE was cocrystallized with D-xylitol 5-phosphate and $ZnCl_2$ as follows. RPE purified as described in the first paragraph of this section (8.9 mg/mL in 10 mM Tris-HCl, pH 7.9) was incubated with 80 mM D-xylitol 5-phosphate and 1 mM $ZnCl_2$ for 30 min at 4 °C. The ternary complex was crystallized by hanging drop vapor diffusion by combining 1 μL of the protein−ligand solution with 1 μL of a reservoir solution containing 19% PEG 3350, 1 mM $ZnCl_2$, 0.1 M succinate, pH 7.0. Crystals appeared in 5−6 days as thin plates and exhibited diffraction consistent with the monoclinic space group $P2_1$ ($a = 80.02$ Å, $b = 199.45$ Å, $c = 87.62$ Å, $\beta = 109.8°$, with 12 molecules of the ternary complex per asymmetric unit). Prior to data collection, the crystals were transferred to a cryoprotectant solution composed of 19% PEG3350, 80 mM D-xylitol 5-phosphate, 1 mM $ZnCl_2$, 0.1 M succinate, pH 7.0, and 30% glycerol and flash-cooled in a nitrogen stream. X-ray diffraction data were collected to 1.8 Å resolution at the NSLS X4A beamline (Brookhaven National Laboratory) on an ADSC CCD detector. Diffraction intensities were integrated and scaled with programs DENZO and SCALEPACK (*30*). The final 1.8 Å data set was 96.9% complete with an R_{merge} of 0.087.

Structure Determination and Model Refinement. The structure of the ternary RPE·D-xylitol 5-phosphate·Zn^{2+} complex was solved by molecular replacement with program EPMR (*31*), using a polyserine search model derived from the *Synechocystis* RPE hexamer (PDB file 1TQJ). Two clear solutions were found using all data between 15 and 4 Å resolution. Rigid body refinement with CNS (*32*) yielded an electron density map with clear features for a number of amino acid side chains in the *S. pyogenes* RPE sequence. The bound D-xylitol 5-phosphate and Zn^{2+} were clearly visible in electron density maps calculated immediately after the first cycle of rigid body refinement of the protein molecule alone. Iterative cycles of manual rebuilding with TOM (*33*) and refinement with CNS resulted in a model with R_{cryst} and R_{free} of 0.224 and 0.256, respectively. The final structure contains 19 748 protein atoms, 12 inhibitor molecules, 12 Zn^{2+} atoms, and 991 water molecules for two hexamers of the complex in the asymmetric unit. All nonglycine residues lie in allowed regions of the Ramachandran plot. X-ray data collection and crystallographic refinement statistics are provided in Table 1.

RESULTS AND DISCUSSION

We previously described the mechanistically distinct OMP decarboxylase suprafamily that unequivocally includes

Table 1: Data Collection and Refinement Statistics

	Data Collection
space group	$P2_1$
cell dimensions	$a = 80.02$ Å, $b = 199.45$ Å, $c = 87.62$ Å, $\beta = 109.76°$
data redundancy	5.1
unique reflections	229 414
resolution (Å)[a]	40−1.8 (1.86−1.80)
completeness (%)[a]	96.9 (88.7)
R_{merge} (%)[a]	8.7 (34.5)
average I/σ[a]	17.4 (3.3)
	Refinement
resolution (Å)	25−1.8
no. of reflections	
working set	209 730
test set	10 427
R_{work}/R_{free} (%)	22.4/25.6
no. of atoms	
protein	19 748
solvent	991
inhibitor	168
Zn	12
average B-factor (Å^2)	27.3
rms deviations	
bond lengths (Å)	0.006
bond angles (deg)	1.19

[a] Numbers in parentheses indicate values for the highest resolution shell.

OMPDC, KGPDC, and HPS: the structurally characterized KGPDC and OMPDC share a conserved dimeric quaternary structure as well as several conserved active site residues, including a characteristic D-x-K-x-x-D motif located at the end of the third β-strand in the $(\beta/\alpha)_8$-barrel (*11*). Although a high-resolution structure is not yet available to an HPS, it certainly is a member of the suprafamily based on the presence of the conserved D-x-K-x-x-D sequence motif and the conserved requirement for stabilization of an enediolate intermediate.

As detailed in the introduction, the SCOP database includes RPE in the "ribulose phosphate binding" superfamily, along with OMPDC and KGPDC. As previously noted, our PSI-BLAST and Shotgun searches of the protein sequence databases using the members of the OMPDC suprafamily as queries confirm that RPE shares sequence homology with the "ribulose phosphate binding" superfamily. In an extreme example, a BLASTP sequence alignment relating the HPS from *Methylomonas aminofaciens* and the RPE from *S. pyogenes* (the subject of this article) is described by a 26% sequence identity throughout the sequences of both proteins. On the basis of these distant relationships, we proposed that RPE is a member of the OMPDC suprafamily (*34*, *35*). However, a more typical result is significant sequence identity only in a segment that corresponds to the conserved C-terminal $(\beta/\alpha)_2$-phosphate binding motif.

Given SCOP's inclusion of RPE with the structurally characterized members of the OMPDC suprafamily despite low levels of sequence identity, we decided that more thorough investigations of the structural and functional properties of RPE were necessary before RPE could be considered a bona fide member of the "ribulose phosphate binding" superfamily, i.e., clearly related to the other members by divergent evolution of the intact $(\beta/\alpha)_8$-barrel fold.

We now report a functional characterization of the RPE from *S. pyogenes* that demonstrates that it requires a divalent metal ion and can be activated by Zn^{2+}; we also report a structural characterization that reveals the geometry of a bound substrate analogue. These observations are interpreted in the context of both the OMPDC suprafamily and the "ribulose-phosphate binding superfamily".

Table 2: Activity[a] and Stoichiometry of Zn^{2+} Binding[b] for Wild Type RPE

sample	k_{cat} (s^{-1})	Zn
as isolated	480 ± 160	0.3
metal-free[d]	100 ± 45	0.1
as isolated + Zn[c]	840 ± 80	0.9
metal-free + Zn[c]	870 ± 80	1.1

[a] Assayed with the polarimetric assay as described in Materials and Methods. [b] Assayed by ICP analysis as described in Materials and Methods [c] 0.5 mM $ZnCl_2$ present in assay. [d] 10 mM EDTA present in assay.

Activation of Wild Type RPE from S. pyogenes by Zn^{2+}. Whether the wild type RPE from *S. pyogenes* was isolated from *E. coli* (1) using the pET17b expression vector (without an N-terminal His-tag) followed by DEAE-chromatography or (2) using the pDMS1a-10His expression vector (with an N-terminal 10 His-tag) followed by purification by a Ni-chelating column and cleavage of the His-tag with thrombin, the divalent metal ion content as measured by ICP analysis was equivalent: ~0.40 equiv of Zn and ~0.2 equiv of Fe per polypeptide. These samples had comparable activities in the spectrophotometric assay. For the studies reported in this manuscript we utilized the Ni-chelating purification procedure, because we were unable to express the H34A and H67A (vide infra) mutants without the His-tag and considered it desirable to isolate all of the proteins using the same procedure.

When wild type RPE was assayed for the production of D-xylulose 5-phosphate from D-ribulose 5-phosphate with the irreversible coupled-enzyme system described in Materials and Methods, the measured values for k_{cat} and K_m for D-ribulose 5-phosphate were 280 ± 50 s^{-1} and 0.2 ± 0.04 mM, respectively. Because divalent metal ions cannot be excluded from the coupled-enzyme assay, we routinely used a polarimeter-based assay in most of our studies to measure the equilibration of D-ribulose 5-phosphate and D-xylulose 5-phosphate. The sensitivity of this assay precludes measurement of values of K_m; however, using 10 mM D-ribulose 5-phosphate (saturating based on the coupled-enzyme assay), the measured value for the "apparent" k_{cat} is 480 ± 160 s^{-1} (Table 2). The difference in the values for the rates measured in the two assays can be explained because the polarimetric assay measures the rate of formation of the equilibrium mixture of D-ribulose 5-phosphate and D-xylulose 5-phosphate. As a result, the value of the "apparent" k_{cat} in the polarimetric assay is the sum of the values of the k_{cat}'s for formation of D-xylulose 5-phosphate from D-ribulose 5-phosphate and for formation of D-ribulose 5-phosphate from D-xylulose 5-phosphate (*29*). In accord with this expectation, the same "apparent" k_{cat} is measured in polarimetric assay when D-xylulose 5-phosphate is used as the substrate. Thus, we conclude that the coupled-enzyme assay and polarimetric assay yield consistent results.

After removal of divalent metal ions from wild type RPE with EDTA as described in the Materials and Methods section, Zn^{2+} is present at stoichiometry of ≤0.10 per

Table 3: Activity[a] of Mutants of RPE

protein	k_{cat} (s^{-1}) +10 mM EDTA[b]	k_{cat} (s^{-1}) +10 μM $ZnCl_2$[c]
H34A	nd[d]	200 ± 7
D36A	nd	nd
H67A	nd	270 ± 60
D176A	nd	nd

[a] Assayed with the polarimetric assay as described in Materials and Methods. [b] 10 mM EDTA present in assay. [c] 10 μM EDTA present in assay. [d] No detectable activity.

polypeptide; Fe^{2+} is not detectable. Using the polarimeteric assay and 10 mM D-ribulose 5-phosphate, the measured value for the "apparent" k_{cat} is 100 ± 45 s^{-1} (Table 2).

After incubation of the "apoenzyme" with a molar excess of Zn^{2+} followed by gel filtration, Zn^{2+} was present at a stoichiometry of 1.0 ion per polypeptide. Using the polarimetric assay, the measured value for the "apparent" k_{cat} was 840 ± 80 s^{-1}.

Incubation of wild type enzyme as isolated with a molar excess of Zn^{2+} followed gel filtration, i.e., without treatment with EDTA, also resulted in a measured occupancy of 1.0 Zn^{2+} ion per polypeptide Again using the polarimetric assay, the measured value for the "apparent" k_{cat} was 870 ± 80 s^{-1}, i.e., equivalent to that attained following incubation with EDTA and addition of Zn^{2+}.

Addition of Mg^{2+} or Fe^{2+} to either the isolated RPE or the "apoenzyme" did not result in activation (data not shown). Although neither Mn^{2+} nor Co^{2+} was detected in purified samples of RPE, both resulted in activation of the "apoenzyme" (data not shown). Because active enzyme with a significant, but incomplete, complement of Zn^{2+} was obtained following purification by DEAE-chromatography (vide supra), we regard Zn^{2+} as the physiologically relevant ion and focused our studies on the catalytic properties of the enzyme activated with Zn^{2+}.

Thus, we conclude that RPE can bind a single Zn^{2+} ion per polypeptide and that catalytic activity can be correlated with the stoichiometry of the bound metal ion.

Metal Ion Content and Catalytic Activity of Mutants of RPE. Although substantial enhancement in activity could be achieved by reconstitution of the "apoenzyme" with excess Zn^{2+}, the samples of "apoenzyme" always retained significant levels of activity (see previous section), presumably due to a high affinity of the binding site for the divalent metal ion. Therefore, we constructed the H34A, D36A, H67A, and D176A mutants; these His and Asp residues are strictly conserved in all RPEs and were observed to coordinate Zn^{2+} in the recently reported structures of the RPE from rice (*18*) and *P. falciparum* (*20*). Without treatment with EDTA and following gel filtration, these mutant RPEs had negligible amounts of bound divalent metal ions and no detectable catalytic activity using the polarimetric assay (Table 3). However, when assayed with the polarimetric assay in the presence of Zn^{2+}, the H34A and H67A mutants displayed substantial activities, with the values of the "apparent" k_{cat}'s measured as 200 ± 10 s^{-1} and 270 ± 60 s^{-1}, respectively, at 10 μM $ZnCl_2$ (higher concentrations were inhibitory). No activity could be detected with the D36A and D176A mutants in the presence of added Zn^{2+}; we attribute this inactivity to the participation of these residues as acid/base catalysts in the 1,1-proton transfer reaction. Furthermore, addition of

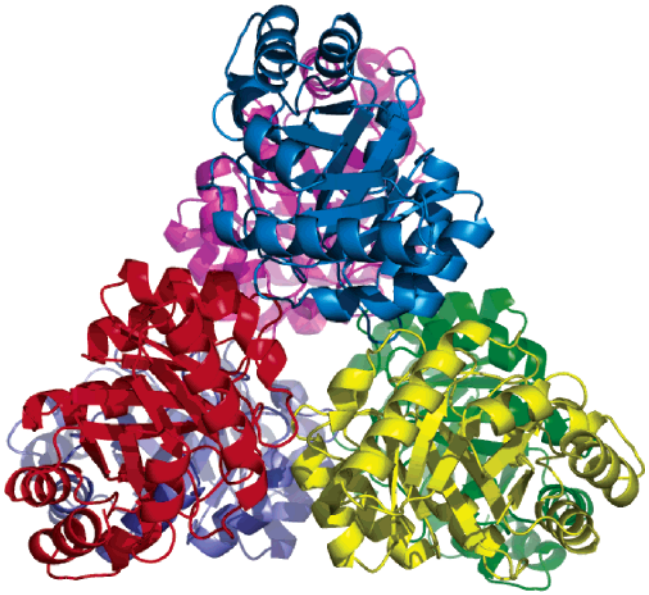

FIGURE 1: The RPE hexamer. The crystallographic asymmetric unit contains two hexamers, for a total of twelve polypeptides. Each hexamer can be described as a trimer of dimers, based on the nature of quaternary contacts between the various polypeptides.

Zn^{2+} to all four of the mutants followed by gel filtration produced proteins with no bound Zn^{2+}. Thus, in contrast to wild type RPE, Ala substitutions for each of the metal ion ligands observed in the structure of the RPE from rice (*18*) significantly reduced the affinity of the active site for Zn^{2+}, although the H34A and H67A mutants could be activated by the presence of Zn^{2+} in the assay.

Based on our ability (1) to produce comparable levels of enhanced activity of wild type RPE either by addition of Zn^{2+} or by initial incubation with EDTA followed by addition of Zn^{2+} and also (2) to obtain inactive, metal-free samples of H34A and H67A and restore substantial levels of activity in the presence of Zn^{2+}, we conclude that RPE requires a divalent metal ion and that Zn^{2+} can serve that function.

Structure of the D-Xylitol 5-Phosphate Complex of RPE from S. pyogenes. As noted previously, the structures of RPEs from potato (*17*), rice (*18*), *Synechocystis* (*19*), and *P. falciparum* (*20*) are available. In each, the component polypeptides share a conserved $(\beta/\alpha)_8$-barrel fold. The RPEs from potato and *Synechocystis* are described by a conserved hexameric quaternary structure; the RPEs from rice and *P. falciparum* are dimers. The hexameric assemblies observed in the former structures are best described as trimers of more tightly associated dimers. The quaternary interactions in the various dimeric structures are conserved.

The RPE from *S. pyogenes* was crystallized in the presence of D-xylitol 5-phosphate, an analogue of D-xylulose 5-phosphate, and $ZnCl_2$, and the structure was solved by molecular replacement at 1.8 Å resolution using the structure of the RPE from *Synechocystis* as the search model. Two hexamers of identical $(\beta/\alpha)_8$-barrels constituted the asymmetric unit, in contrast to the single hexamers that constituted the asymmetric units for the RPEs from potato and *Synechocystis* (Figure 1). The quaternary structure can be described as a trimer of dimers.

Mechanism of the RPE-Catalyzed Reaction. The structure of the active site of liganded RPE from *S. pyogenes* closely

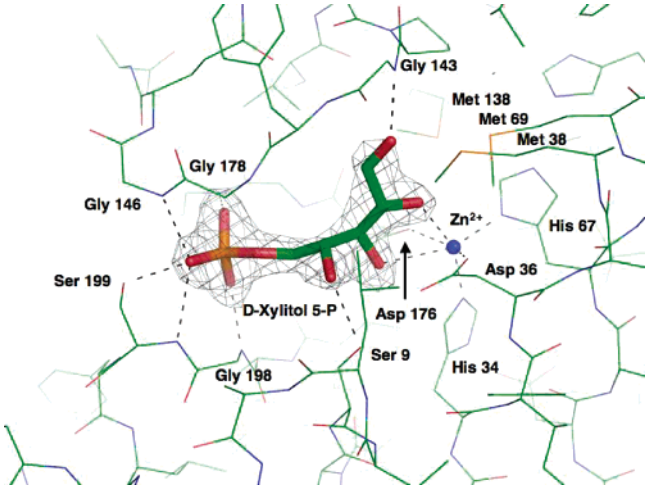

FIGURE 2: View of the active site of RPE and representative electron density for D-xylitol 5-phosphate. The electron density was obtained from a $F_o - F_c$ omit map contoured at 1σ. The details of the interactions between the substrate analogue and active site are described in the text.

resembles those previously determined for the RPEs from potato, rice, *Synechocystis*, and *P. falciparum*. However, in the present structure an octahedrally coordinated Zn^{2+} ion is located in the active site (Figure 2). The ligands are Nδ of His 34, Nϵ of His 67, one carboxylate oxygen from both Asp 36 and Asp 176, and the O2 and O3 of the D-xylitol 5-phosphate ligand.

Conserved hydrogen-bonding interactions involving both His 34 (to Asp 65) and His 67 (to His 91) position these residues for their roles as ligands to the Zn^{2+}. In such a spatial configuration, it is unlikely that His 34 and His 67 would be protonated. Thus, these residues are not expected to be involved in catalysis via hydrogen-bonding interactions with the bound substrate and the 2,3-enediolate intermediate that is expected to be present on the reaction coordinate.

In addition to its interactions of the substrate analogue with the Zn^{2+}, the substrate is bound to the protein via hydrogen bonding interactions between O1 and the backbone amide of Gly 143, O4 and the hydroxyl group of Ser 9, and the phosphate group and four backbone amides. Three of the latter interactions, those associated with Gly 178, Gly 198, and Ser 199, are located in the commonly observed, conserved phosphate binding motif located at the ends of the seventh and eighth β-strands in $(\beta/\alpha)_8$-barrel enzymes (*21*). The fourth, associated with Gly 146, is located on a loop that is inserted between the end of the sixth β-strand and the beginning of the sixth α-helix. This loop is ordered and closed in structures of the unliganded RPEs from potato and *P. falciparum* that were crystallized in the presence of inorganic sulfate; this phosphate mimic is also located in the phosphate binding sites at the ends of the seventh and eighth β-strands and forms hydrogen bonds to the conserved NH groups of Gly residues. The analogous loops are in an open conformation in the RPE from rice and disordered in the RPE from *Synechocystis*; the crystals used to determine both of these structures were obtained in the absence of sulfate or phosphate. Because the phosphate binding site is unoccupied in the latter structures, the critical hydrogen bonding interaction of an anionic ligand with the backbone amide in the loop is not possible, so closure of the loop is not favored.

From this structure, the mechanism of the 1,1-proton transfer reaction and the role of Zn^{2+} in catalysis immediately follow (Figure 3). Proton abstraction from carbon-3 of either D-ribulose 5-phosphate (by Asp 36) or D-xylulose 5-phosphate (by Asp 176) generates an anionic 2,3-enediolate intermediate. The Zn^{2+} ion stabilizes the otherwise kinetically incompetent intermediate through electrostatic interactions with the anionic oxygen located on carbon-2. Protonation of the intermediate by Asp 176 yields D-xylulose 5-phosphate. In the reverse direction (conversion of D-ribulose 5-phosphate to D-xylulose 5-phosphate), the roles of the Asp residues would be reversed.

Although Asp 36 and Asp 176 are also ligands of the Zn^{2+} ion in the hexacoordinate complex with D-xylitol 5-phosphate, no other potential acid/base catalysts can be identified in the active site. Presumably, as postulated for the reaction catalyzed by glyoxalase I, which has a similar active site structure and also catalyzes proton abstraction to yield a metal ion-coordinated enediolate intermediate (*36*), the carboxylate group of Asp 36 or Asp 176 can dissociate from the inner coordination sphere of the essential Zn^{2+} ion, allowing either proton abstraction from the substrate or protonation of the intermediate by a solvent-derived proton. The active site contains ordered water molecules proximal to both carboxylate groups that may shuttle protons from the solvent to the active site. Our observation that the D36A and D176A mutants are devoid of catalytic activity and cannot be activated by exogenous Zn^{2+} is consistent with their participation as the acid/base catalysts.

A summary of the essential details of the reactions catalyzed by OMPDC, KGPDC, and RPE is shown in Figure 4. The reaction catalyzed by OMPDC is metal-independent, that catalyzed by KGPDC is Mg^{2+}-dependent, and that catalyzed by RPE is Zn^{2+}-dependent. The reaction catalyzed by OMPDC likely avoids a vinyl anion intermediate; the reaction catalyzed by KGPDC involves a 1,2-enediolate intermediate stabilized by coordination of oxygens-2 and -3 to its metal ion; and the reaction catalyzed by RPE involves a 2,3-enediolate intermediate also stabilized by coordination of oxygens-2 and -3 to its metal ion.

Relationship of RPE to the OMPDC Suprafamily: Active Site Structure. A comparison of the active sites of OMPDC (1DBT from *Bacillus subtilis* with the 5′-UMP product bound in the active site), KGPDC (1Q6L with Mg^{2+} and L-threonohydroxamate 4-phosphate, an analogue of the enediolate intermediate, bound in the active site), and the RPE from *S. pyogenes* (with Zn^{2+} and D-xylitol 5-phosphate bound in the active site) is shown in Figure 5. The positions of the bound ligands are remarkably similar; in addition, the positions of the Mg^{2+} in KGPDC and the Zn^{2+} in RPE are also remarkably similar. Presumably the similar locations of the bound ligands are dictated by (1) the positions of the conserved phosphate binding sites at the ends of the seventh and eighth β-strands in the $(\beta/\alpha)_8$-barrels (Gly 214 and Arg 215 in OMPDC; Gly 171, Gly 191, and Arg 192 in KGPDC; and Gly 178, Gly 198, and Ser 199 in RPE) and (2) the requirement that the acid/base functional groups, as well as the ligands for the metal ions in KGPDC and RPE, be located at the ends of the remaining β-strands.

Figure 5 also details the positions of the various amino acid functional groups that have been implicated in the OMPDC-, KGPDC-, and RPE-catalyzed reactions. The three

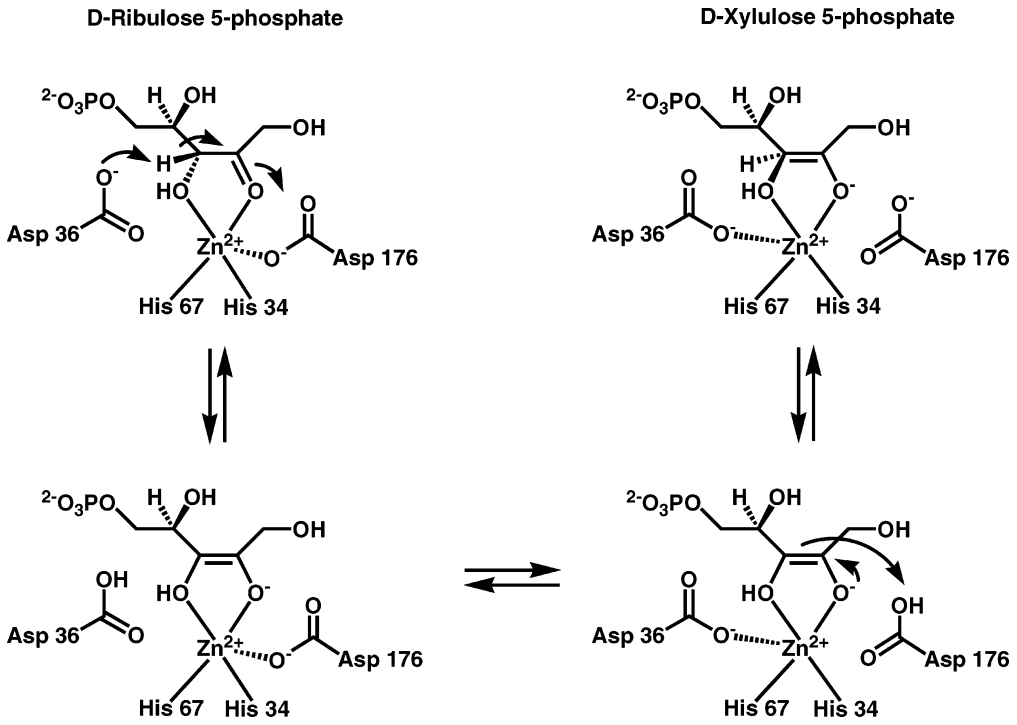

FIGURE 3: Mechanism of the RPE-catalyzed reaction based on the structure of the D-xylitol 5-phosphate·Zn^{2+} complex.

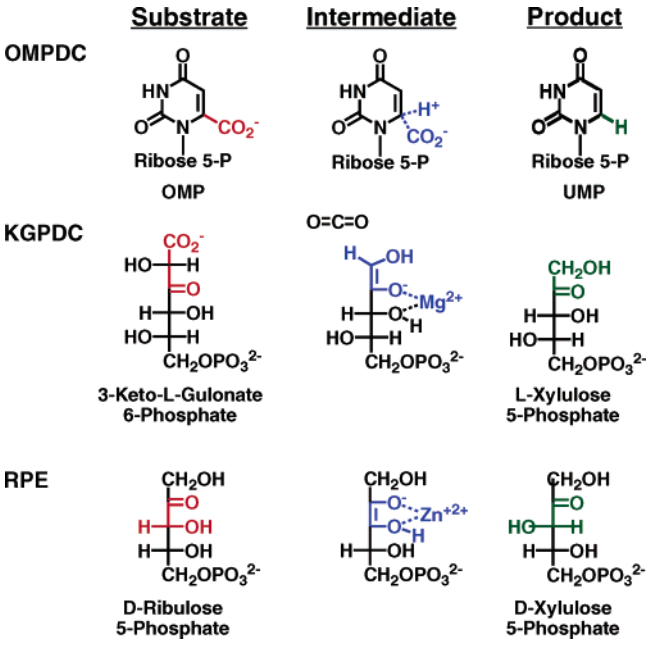

FIGURE 4: Summary of the mechanisms of the reactions catalyzed by RPE, OMPDC, and KGPDC. The colors highlight the differing structures of the substrates (red), intermediates (blue), and products (green).

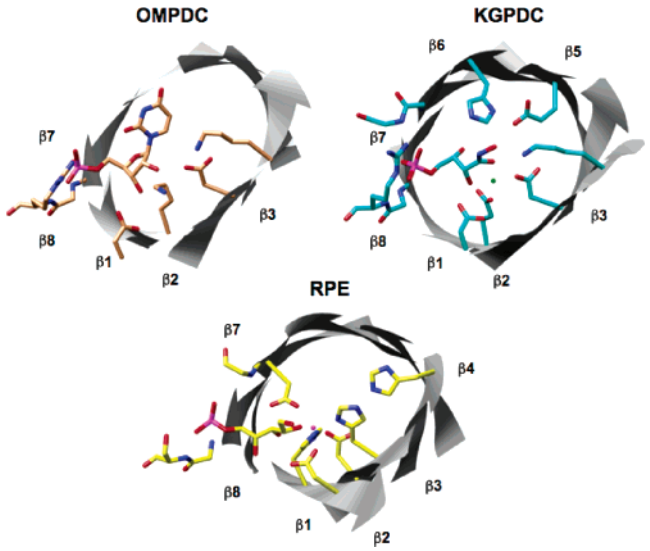

FIGURE 5: A comparison of the active site structures of OMPDC (1DBT from *Bacillus subtilis* with 5′-UMP product bound in the active site), KGPDC (1Q6L with L-threonohydroxamate 4-phosphate, an analogue of the enediolate intermediate bound in the active site), and the RPE from *S. pyogenes* (with D-xylitol 5-phosphate bound in the active site). The identities of the active site residues are as follows. OMPDC: β-strand 1, Asp 11; β-strand 2, Lys 33; and β-strand 3, Asp 60 and Lys 62. KGPDC: β-strand 1, Asp 11; β-strand 2, Glu 33; β-strand 3, Asp 62 and Lys 64; β-strand 5, Glu 112; and β-strand 6, His 136. RPE: β-strand 2, His 34 and Asp 36, β-strand 3, Asp 65 and His 67; β-strand 4, His 91; and β-strand 7, Asp 176. In each active site, the phosphate group of the bound ligand interacts with peptide backbone NH-groups at the ends of the β-strands 7 and 8.

active sites have structurally conserved but nonidentical groups at the ends of the second β-strand (Lys 33 in OMPDC, Glu 33 in KGPDC, and both His 34 and Asp 36 in RPE) and third β-strand (Asp 60 in OMPDC, Asp 62 in KGPDC, and His 67 in RPE). However, none of the remaining functional groups are positionally shared by all three active sites. That the structurally conserved groups at the ends of the second and third β-strands are not identical could be the result of divergent evolution; however, an alternate explanation is that in $(\beta/\alpha)_8$-barrels the positions of functional groups are restricted to the ends of the various β-strands, so the "conserved" positions of these functional groups are a requirement of structure and not divergent evolution of function. Furthermore, we believe that it is noteworthy that none of the metal ion ligands or acid/base catalysts in the active sites of OMPDC, KGPDC, and RPE are conserved.

Relationship of RPE to the OMPDC Suprafamily: Quaternary Structure. As noted in the introduction, proteins that share the $(\beta/\alpha)_8$-barrel fold have the same topology. As expected, a DALI search (*37*; http://www.ebi.ac.uk/dali/) of the protein structure database using the structure of the RPE from *S. pyogenes* as query yields many homologous structures, all of which share the $(\beta/\alpha)_8$-barrel fold. Among the top scoring structures are (1) pyridoxine 5-phosphate synthase from *E. coli* (1HO1; $Z = 18.1$), (2) indole-3-glycerophosphate synthase from *Sulfolobus solfataricus* (1A53; $Z = 18.1$; "ribulose phosphate binding" superfamily), (3) *N*-(5′-phosphoribosyl)anthranilate isomerase from *E. coli* (1PII; $Z = 18.0$; "ribulose phosphate binding" superfamily), (4) OMPDC from *Methanobacterium thermoautotrophicum* (1DVJ; $Z = 17.9$; "ribulose phosphate binding" superfamily), (5) imidazoleglycerolphosphate synthase from *Thermotoga maritima* (1THF; $Z = 17.8$; "ribulose phosphate binding" superfamily), (6) phosphoribosylformimino-5-aminoimidazole carboxamide ribotide isomerase from *Thermotoga maritima* (1NSJ; $Z = 16.9$; "ribulose phosphate binding" superfamily), (7) triose phosphate isomerase from *Pyrococcus woesi* (1HG3; $Z = 16.7$), and (8) KGPDC from *E. coli* (1KV8; $Z = 16.5$; "ribulose phosphate binding" superfamily). Although this list includes all of the members of the "ribulose phosphate binding" superfamily, it also includes two that are not (pyridoxine 5-phosphate synthase and a triose phosphate isomerase) but contain the commonly observed phosphate binding motif located at the ends of the seventh and eighth β-strands of the $(\beta/\alpha)_8$-barrel fold. Accordingly, we do not believe that topology of the $(\beta/\alpha)_8$-barrel fold is sufficient evidence to conclude that RPE is related to OMPDC and KGPDC by divergent evolution from a common ancestor. The results of ongoing sequence and structure-based analyses of the entire SCOP "ribulose phosphate binding" superfamily are consistent with this conclusion (W. R. P. Novak, J. A. Gerlt, and P. C. Babbitt, in preparation); these will be reported soon.

We believe that additional structural evidence relevant to the question of whether OMPDC, KGPDC, and RPE diverged from a common ancestor can be obtained from consideration of the quaternary interactions between the polypeptides in their dimeric structures. The dimeric structures are compared in Figures 6 and 7. As shown in Figure 6, using one polypeptide of the dimer as the reference for superposition in which the various β-strands in the $(\beta/\alpha)_8$-barrels are superimposed in sequence from the N- to C-termini, both polypeptides of the dimer OMPDC and KGPDC superimpose as expected given their homologous relationship. However, the second polypeptide of RPE does not superimpose on the second polypeptide of either OMPDC or KGPDC. This is a consequence of the quaternary interactions involving spatially different contacts between the component polypeptides.

In OMPDC, the canonical second, third, fourth, and fifth α-helices as well as extrabarrel helices inserted following the sixth and seventh β-strands are involved in extensive interpolypeptide contacts; a view along the 2-fold axis that relates the polypeptides of the dimer is shown in Figure 7. In KGPDC, the canonical second, third, and fourth α-helices as well as an extrabarrel helix inserted following the sixth β-strand are involved in somewhat less extensive, but still substantial, interpolypeptide contacts. As a consequence of the geometry of these contacts, in both OMPDC and KGPDC the active sites are shared between the two polypeptides, with an Asp in the loop that connects the third β-strand and third α-helix (in the conserved D-x-K-x-x-D motif) penetrating into and completing the active site that is otherwise formed by the other polypeptide. We earlier used the conserved details of the shared active sites to argue that OMPDC and KGPDC are homologues, despite the distinct mechanisms of the decarboxylation reactions they catalyze.

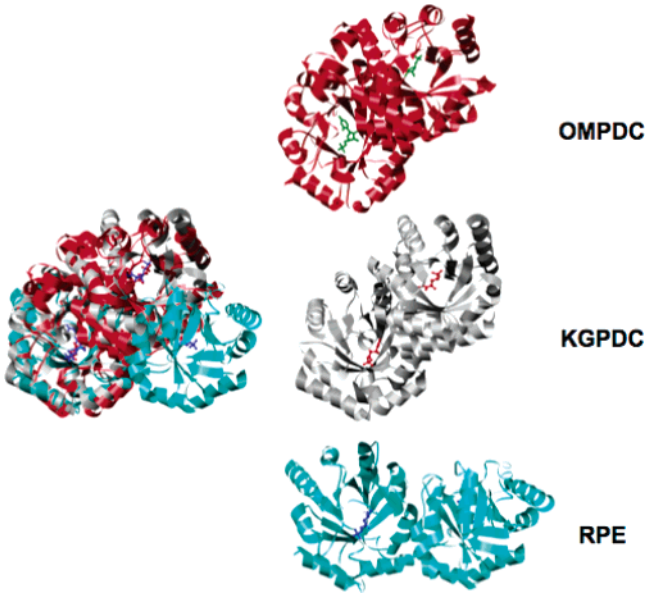

FIGURE 6: Left panel, a superposition of the dimers of OMPDC (red), KGPDC (gray), and REP (cyan); right panel, the separated dimers retaining the orientations in the left panel.

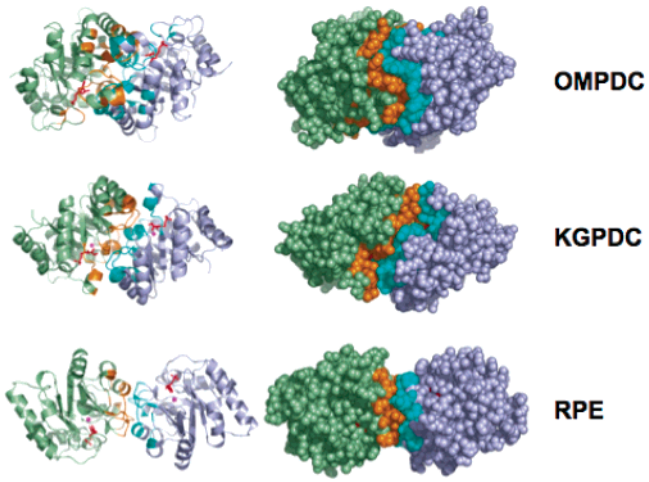

FIGURE 7: The dimers of OMPDC (top), KGPDC (middle), and RPE (bottom) viewed down the 2-fold axis showing the similar polypeptide interfaces in OMPDC and KGPDC and the differing polypeptide interface in RPE. The portions of the component polypeptides of the dimer that are within 4 Å of the interface are shaded in orange and cyan.

However, in RPE, the canonical second, third, and fourth α-helices are involved in less extensive interpolypeptide contacts (Figure 7). As a result of the differing contacts, the component polypeptides have different orientations than those that are conserved in the OMPDC and KGPDC dimers. In contrast to both OMPDC and KGPDC, each active site of RPE is contained entirely within a single polypeptide.

We view the differing quaternary relationships of the polypeptides in the RPE dimer as additional evidence that RPE is not the result of divergent evolution of the intact $(\beta/\alpha)_8$-barrel from the common ancestor from which OMPDC and KGPDC diverged, despite the observation that they share the $(\beta/\alpha)_8$-barrel fold.

Summary and Conclusions. The reaction catalyzed by OMPDC is metal-independent; the reactions catalyzed by both HPS and KGPDC are Mg^{2+}-dependent. We have demonstrated that the RPE-catalyzed reaction is also divalent metal ion dependent and can be activated by Zn^{2+}. The structure of the D-xylitol 5-phosphate liganded complex allows the suggestion that the divalent metal ion stabilizes a 2,3-enediolate intermediate produced by abstraction of the 3-proton from either D-ribulose 5-phosphate (by Asp 36 at the end of the second β-strand) or D-xylulose 5-phosphate (by Asp 176 at the end of the seventh β-strand). The metal ion is coordinated to these functional groups as well as His 34 at the end of the second β-strand and His 67 at the end of the third β-strand. Although both OMPDC and KGPDC contain essential functional groups at the ends of the second and third β-strands, their identities are not conserved. Furthermore, the active sites of OMPDC, KGPDC, and RPE contain functional groups that are unique to each reaction. And, finally, although OMPDC, KGPDC, and RPE are dimers of $(\beta/\alpha)_8$-barrels, the quaternary interactions are distinct. As a result of these functional and structural differences, we conclude that RPE should not be considered a member of the OMPDC suprafamily.

However, RPE does share the phosphate binding motif located at the ends of the seventh and eighth β-strands of the $(\beta/\alpha)_8$-barrel fold found in the bona fide members of the OMPDC suprafamily as well as in many other $(\beta/\alpha)_8$-barrel enzymes that bind phosphorylated substrates; the latter include, but are not restricted to, those that constitute the members of SCOP's "ribulose phosphate binding" superfamily. As a result, our functional and structural analyses support the hypothesis that many $(\beta/\alpha)_8$-barrel enzymes that bind phosphorylated substrates evolved via construction of a complete $(\beta/\alpha)_8$-barrel from $(\beta/\alpha)_{2N}$-fractional barrels (where $N = 1$, 2, or 3), including C-terminal $(\beta/\alpha)_2$-quarter barrel that provides the phosphate binding motif (*22*, *23*). If this combinatorial pathway for evolution of structure and function is correct, it is misleading to group RPE, the OMPDC suprafamily, and selected other proteins that share the phosphate binding motif into a single "ribulose phosphate binding" superfamily; such association implies a direct pathway for divergent evolution of its members from a common $(\beta/\alpha)_8$-barrel progenitor. Instead, like the triose phosphate isomerase and D-ribulose 1,5-bisphosphate carboxylase superfamilies, the RPE superfamily and the OMPDC suprafamily should be considered distinct "superfamilies" within the SCOP database. The various superfamilies whose members bind phosphorylated substrates may share a common, C-terminal $(\beta/\alpha)_2$-quarter barrel, but the complete $(\beta/\alpha)_8$-barrels are not the products of divergent evolution from a common ancestor.

REFERENCES

1. Nagano, N., Orengo, C. A., and Thornton, J. M. (2002) One fold with many functions: the evolutionary relationships between TIM barrel families based on their sequences, structures and functions, *J. Mol. Biol. 321*, 741−65.
2. Wierenga, R. K. (2001) The TIM-barrel fold: a versatile framework for efficient enzymes, *FEBS Lett. 492*, 193−8.
3. Gerlt, J. A., and Raushel, F. M. (2003) Evolution of function in (beta/alpha)(8)-barrel enzymes, *Curr. Opin. Chem. Biol. 7*, 252−64.
4. Hocker, B., Beismann-Driemeyer, S., Hettwer, S., Lustig, A., and Sterner, R. (2001) Dissection of a (betaalpha)8-barrel enzyme into two folded halves, *Nat. Struct. Biol. 8*, 32−6.
5. Lang, D., Thoma, R., Henn-Sax, M., Sterner, R., and Wilmanns, M. (2000) Structural evidence for evolution of the β/α barrel scaffold by gene duplication and fusion, *Science 289*, 1546−50.
6. Jurgens, C., Strom, A., Wegener, D., Hettwer, S., Wilmanns, M., and Sterner, R. (2000) Directed evolution of a $(\beta\alpha)$8-barrel enzyme to catalyze related reactions in two different metabolic pathways, *Proc. Natl. Acad. Sci. U.S.A. 97*, 9925−30.
7. Sievers, A., and Wolfenden, R. (2002) Equilibrium of formation of the 6-carbanion of UMP, a potential intermediate in the action of OMP decarboxylase, *J. Am. Chem. Soc. 124*, 13986−7.
8. Miller, B. G., and Wolfenden, R. (2002) Catalytic proficiency: the unusual case of OMP decarboxylase, *Annu. Rev. Biochem. 71*, 847−85.
9. Gao, J. (2003) Catalysis by enzyme conformational change as illustrated by orotidine 5′-monophosphate decarboxylase, *Curr. Opin. Struct. Biol. 13*, 184−92.
10. Hur, S., and Bruice, T. C. (2002) Molecular dynamic study of orotidine-5′-monophosphate decarboxylase in ground state and in intermediate state: a role of the 203-218 loop dynamics, *Proc. Natl. Acad. Sci. U.S.A. 99*, 9668−73.
11. Wise, E., Yew, W. S., Babbitt, P. C., Gerlt, J. A., and Rayment, I. (2002) Homologous (beta/alpha)8-barrel enzymes that catalyze unrelated reactions: orotidine 5′-monophosphate decarboxylase and 3-keto-L-gulonate 6-phosphate decarboxylase, *Biochemistry 41*, 3861−9.
12. Wise, E., Yew, W. S., Gerlt, J. A., and Rayment, I. (2003) Structural evidence for a 1,2-enediolate intermediate in the reaction catalyzed by 3-keto-L-gulonate 6-phosphate decarboxylase, a member of the orotidine 5′-monophosphate decarboxylase suprafamily, *Biochemistry 42*, 12133−42.
13. Wise, E. L., Yew, W. S., Gerlt, J. A., and Rayment, I. (2004) Evolution of Enzymatic Activities in the Orotidine 5′-Monophosphate Decarboxylase Suprafamily: Crystallographic Evidence for a Proton Relay System in the Active Site of 3-Keto-l-gulonate 6-Phosphate Decarboxylase, *Biochemistry 43*, 6438−46.
14. Yew, W. S., Wise, E. L., Rayment, I., and Gerlt, J. A. (2004) Evolution of Enzymatic Activities in the Orotidine 5′-Monophosphate Decarboxylase Suprafamily: Mechanistic Evidence for a Proton Relay System in the Active Site of 3-Keto-l-gulonate 6-Phosphate Decarboxylase, *Biochemistry 43*, 6427−37.
15. Wise, E. L., Yew, W. S., Gerlt, J. A., and Rayment, I. (2003) Structural evidence for a 1,2-enediolate intermediate in the reaction catalyzed by 3-keto-L-gulonate 6-phosphate decarboxylase, a member of the orotidine 5′-monophosphate decarboxylase suprafamily, *Biochemistry 42*, 12133−42.
16. Chen, Y. R., Larimer, F. W., Serpersu, E. H., and Hartman, F. C. (1999) Identification of a catalytic aspartyl residue of D-ribulose 5-phosphate 3-epimerase by site-directed mutagenesis, *J. Biol. Chem. 274*, 2132−6.
17. Kopp, J., Kopriva, S., Suss, K. H., and Schulz, G. E. (1999) Structure and mechanism of the amphibolic enzyme D-ribulose-5-phosphate 3-epimerase from potato chloroplasts, *J. Mol. Biol. 287*, 761−71.
18. Jelakovic, S., Kopriva, S., Suss, K. H., and Schulz, G. E. (2003) Structure and catalytic mechanism of the cytosolic D-ribulose-5-phosphate 3-epimerase from rice, *J. Mol. Biol. 326*, 127−35.
19. Wise, E. L., Akana, J., Gerlt, J. A., and Rayment, I. (2004) Structure of D-ribulose 5-phosphate 3-epimerase from Synechocystis to 1.6 Å resolution, *Acta Crystallogr., Sect. D: Biol. Crystallogr. 60*, 1687−90.
20. Caruthers, J., Bosch, J., Buckner, F., Van Voorhis, W., Myler, P., Worthey, E., Mehlin, C., Boni, E., Detitta, G., Luft, J., Lauricella, A., Kalyuzhniy, O., Anderson, L., Zucker, F., Soltis, M., and Hol, W. G. (2006) Structure of a ribulose 5-phosphate 3-epimerase from Plasmodium falciparum, *Proteins 62*, 338−42.
21. Bork, P., Gellerich, J., Groth, H., Hooft, R., and Martin, F. (1995) Divergent evolution of a beta/alpha-barrel subclass: detection of numerous phosphate-binding sites by motif search, *Protein Sci. 4*, 268−74.

22. Henn-Sax, M., Hocker, B., Wilmanns, M., and Sterner, R. (2001) Divergent evolution of (betaalpha)8-barrel enzymes, *Biol. Chem. 382*, 1315−20.
23. Gerlt, J. A., and Babbitt, P. C. (2001) Barrels in pieces?, *Nat. Struct. Biol. 8*, 5−7.
24. Datsenko, K. A., and Wanner, B. L. (2000) One-step inactivation of chromosomal genes in *Escherichia coli* K-12 using PCR products, *Proc. Natl. Acad. Sci. U.S.A. 97*, 6640−45.
25. Schmidt, D. M., Mundorff, E. C., Dojka, M., Bermudez, E., Ness, J. E., Govindarajan, S., Babbitt, P. C., Minshull, J., and Gerlt, J. A. (2003) Evolutionary potential of (beta/alpha)8-barrels: functional promiscuity produced by single substitutions in the enolase superfamily, *Biochemistry 42*, 8387−93.
26. McCall, K. A., and Fierke, C. A. (2000) Colorimetric and fluorimetric assays to quantitate micromolar concentrations of transition metals, *Anal. Biochem. 284*, 307−15.
27. Yew, W. S., Akana, J., Wise, E. L., Rayment, I., and Gerlt, J. A. (2005) Evolution of enzymatic activities in the orotidine 5′-monophosphate decarboxylase suprafamily: enhancing the promiscuous D-arabino-hex-3-ulose 6-phosphate synthase reaction catalyzed by 3-keto-L-gulonate 6-phosphate decarboxylase, *Biochemistry 44*, 1807−15.
28. Kiely, M. E., Stuart, A. L., and Wood, T. (1973) Partial purification and kinetic properties of ribose-5-phosphate ketol-isomerase and ribulose-5-phosphate 3-epimerase from various sources, *Biochim. Biophys. Acta 293*, 534−41.
29. Jencks, W. P. (1969) *Catalysis in Chemistry and Enzymology*, pp 586−589, McGraw-Hill Book Company, New York.
30. Otwinowski, Z., and Minor, W. (1997) Processing of X-ray diffraction data collected in oscillation mode, in *Methods in Enzymology* (Carter, C. W. J., Sweet, R. M., Abelson, J. N., and Simon, M. I., Eds.) pp 307−326, Academic Pres, New York.
31. Kissinger, C. R., Gehlhaar, D. K., and Fogel, D. B. (1999) Rapid automated molecular replacement by evolutionary search, *Acta Crystallogr., Sect. D: Biol. Crystallogr. 55* (Part 2), 484−91.
32. Brunger, A. T., Adams, P. D., Clore, G. M., DeLAno, W. L., Gros, P., Grosse-Kunstleve, R. W., Jiang, J. S., Kuszewski, J., Nilges, M., Pannu, N. S., Read, R. J., Rice, L. M., Simonson, T., and Warren, G. L. (1998) Crystallography & NMR system: A new software suite for macromolecular structure determination, *Acta Crystallogr. D54*, 905−21.
33. Jones, A. T. (1985) Interactive computer graphics: FRODO, *Methods Enzymol. 115*, 157−71.
34. Gerlt, J. A., and Babbitt, P. C. (2001) DIVERGENT EVOLUTION OF ENZYMATIC FUNCTION: Mechanistically Diverse Superfamilies and Functionally Distinct Suprafamilies, *Annu. Rev. Biochem. 70*, 209−46.
35. Wise, E. L., and Rayment, I. (2004) Understanding the importance of protein structure to nature's routes for divergent evolution in TIM barrel enzymes, *Acc. Chem. Res. 37*, 149−58.
36. Cameron, A. D., Ridderstrom, M., Olin, B., Kavarana, M. J., Creighton, D. J., and Mannervik, B. (1999) Reaction mechanism of glyoxalase I explored by an X-ray crystallographic analysis of the human enzyme in complex with a transition state analogue, *Biochemistry 38*, 13480−90.
37. Holm, L., and Sander, C. (1995) Dali: a network tool for protein structure comparison, *Trends Biochem. Sci. 20*, 478−80.

BI052474M